Locally Optimal Inspired Detection in Snapping Shrimp Noise

Ahmed Mahmood, *Member, IEEE*, Mandar Chitre, *Senior Member, IEEE*, and Hari Vishnu, *Member, IEEE*

***Abstract*—In this paper, we address the problem of detecting a known signal in snapping shrimp noise. The latter dominates the ambient soundscape at medium-to-high frequencies in warm shallow waters. The noise process is impulsive, exhibits memory and is modeled effectively by stationary α-sub-Gaussian noise with memory order m (αSGN(m)), which is essentially an impulsive Markov process. Robust detectors have long been used to mitigate the impact of impulsive noise on the performance of digital systems. However, conventional notions of robustness do not assume memory within the noise process. The αSGN(m) model offers a mathematical model to develop robust detectors that also exploit the mutual information between noise samples. Recent works in this area highlight substantial improvement in detection performance over traditional robust methods in snapping shrimp noise. However, implementing such detectors is a challenge as they are parametric and computationally taxing. To achieve more realizable detectors, we derive the locally optimal detector for αSGN(m). From it, we introduce the generalized memory-based sign correlator and its variants, all of which offer near-optimal performance in αSGN(m). The proposed detectors offer excellent performance in snapping shrimp noise and low computational complexity. These properties make them attractive for use in underwater acoustical systems operating in snapping shrimp noise.**

***Index Terms*—αSGN(m), impulsive noise, Markov process, signal detection, snapping shrimp noise.**

I. Introduction

THE warm shallow acoustical underwater channel exhibits a number of physical features that can be detrimental to the performance of acoustic systems operating within [1]–[3]. One of these features is the ambient noise process, which is dominated by snapping shrimp noise at frequencies greater than 2 kHz [4]. Within this regime, the noise is determinedly non-Gaussian with impulsive characteristics [3], [5]. Moreover, the impulses tend to cluster together due to the memory of the process [3], [6], [7]. Snapping shrimp noise is thus both an impulsive and bursty process. We are interested in detecting signals in snapping shrimp noise. The problem arises in scenarios such as sonar signal processing and packet (preamble) detection in underwater acoustical transceivers deployed in warm shallow waters.

Robust methods have long been used to mitigate the detrimental impact of impulsive noise and interference on the performance of digital systems [8]–[10]. In line with [9], we employ the term robustness to signify a system's resistance to outliers found in impulsive noise. However, the majority of these methods are built on the assumption of independent and identically distributed (IID) samples. We term this notion of robustness as conventional. In reality, as with snapping shrimp noise, closely spaced noise samples are generally dependent [6]. Though conventional robust techniques do not exploit the memory, they offer substantial improvement over methods optimized for Gaussian noise [10]. However, the performance can be enhanced significantly further if the employed methods are robust and consider mutual information between the noise samples [11], [12].

In the literature, several heavy-tailed processes have been employed to model snapping shrimp noise [3], [5]. Of these, the stationary α-sub-Gaussian noise with memory order m (αSGN(m)) model characterizes the temporal amplitude statistics of the latter extremely well and is sufficiently motivated in our previous works [6], [11], [13]. The αSGN(m) model is derived from the stable distribution family and is essentially an impulsive Markov process of order m. Within the framework of this model, optimal and near-optimal detectors for known signals were derived in [11], [13]. These were shown to significantly outperform conventional robust detectors in snapping shrimp noise. Specifically, [13] compares performance of the clairvoyant log-likelihood ratio (LLR) detector for white symmetric α-stable noise (WSαSN) and αSGN(m) in snapping shrimp noise. The WSαSN process consists of IID symmetric α-stable (SαS) samples and is statistically equivalent to αSGN(0) [6], [10]. A detector is termed clairvoyant if it has perfect knowledge of signal strength and parameters of the underlying model [14]. Of the considered detectors, the one corresponding to αSGN(m) offers substantially better performance than that of WSαSN. Unfortunately, memory exploiting robust detectors come with significant computational overhead. The LLR detector, for example, requires estimates of signal strength and the $m+1$ parameters that define the αSGN(m) process for it to be of practical use [11], [14]. Moreover, the LLR detector cannot be expressed in closed form and needs to be evaluated numerically every time. In [11], the latter issue was resolved by proposing good closed-form approximations that offer near-optimal performance. However, the mathematical form of these

Manuscript received January 7, 2017; revised May 19, 2017; accepted July 16, 2017. Date of publication August 11, 2017; date of current version October 11, 2017. *(Corresponding author: Ahmed Mahmood.)*

Guest Editor: J. Alves.

A. Mahmood and H. Vishnu are with the Acoustic Research Laboratory, Tropical Marine Science Institute, National University of Singapore, Singapore 119227 (e-mail: ahmed@arl.nus.edu.sg; hari@arl.nus.edu.sg).

M. Chitre is with the Department of Electrical and Computer Engineering, Acoustic Research Laboratory, Tropical Marine Science Institute, National University of Singapore, Singapore 119227 (e-mail: mandar@arl.nus.edu.sg).

Digital Object Identifier 10.1109/JOE.2017.2731058

detectors and their dependence on parameter estimates make them unattractive for real-time implementation.

In [5], the nonparametric sign correlator (SC) was shown to offer great performance in snapping shrimp noise. The Neyman–Pearson (NP) formulation was employed and the optimal detector was defined as the maximum-likelihood (ML) estimate of signal strength under the assumption of WSαSN. The SC finds its roots within the theory of locally optimal detection in impulsive noise with IID samples [8]. Its simple implementation and robust performance in snapping shrimp noise makes it an attractive prospect when real-time computations are required. Though the SC offers acceptable performance versus complexity tradeoff, it does not exploit the dependence within snapping shrimp noise samples. The primary objective of this work is to derive robust detectors in snapping shrimp noise that depend on a smaller set of model/signal parameters (preferably none) but still exploit memory of the process. By doing so, we hope to achieve computationally simple forms that offer better performance than the SC, yet still perform at par with the αSGN(m) LLR detector in snapping shrimp noise.

Our contributions are listed as follows: We model the detection problem as a binary hypothesis test under the NP framework and derive the locally optimal detector (LOD) for αSGN(m). Its performance is investigated and severe degradation at high signal-to-noise ratio (SNR) is observed. Taking advantage of its form, we propose a new semiparametric detector, namely, the generalized memory-based SC (GMSC). The latter is robust in impulsive noise, exploits dependence between the samples and simplifies to the SC for $m = 0$. Moreover, it is computationally less demanding than the LLR detector for αSGN(m). The GMSC is analyzed in αSGN(m) and recorded snapping shrimp noise data. Performance is compared against the clairvoyant LLR detector and the SC. We further propose the isotropic sign correlator (ISC), which is a special case of the GMSC and essentially nonparametric. The latter characteristic offers a relatively simpler form. Our results highlight that the GMSC and ISC offer a good compromise between performance and computational complexity. In fact, both detectors offer *several* decibels gain over the SC in snapping shrimp noise. We also propose related variants, namely, the prefiltered ISC (pISC) and the prefiltered SC (pSC), and also investigate their respective performances in αSGN(m) and snapping shrimp noise. A list of acronyms is provided in Table I.

Our detection model considers a relatively simple additive noise model and does not consider underwater acoustical channel. The reason for doing so stems primarily from the fact that there is no consensus on a general channel model for underwater acoustical communication [2], as different models are suitable for different environments. Consequently, performance in one scenario does not translate easily to another. Moreover, we are interested in the case where the receiver has no or imperfect channel information, and would like our detectors to be somewhat robust to mismatch in the channel model. To ensure that they indeed work well in a realistic underwater channel, we have included simulation results for an instance of the latter. The overall detection performance deteriorates due to the channel, but

TABLE I
LIST OF ACRONYMS

Acronym	Definition
LOD	locally optimal detector
mLOD	modified locally optimal detector
LLR	log-likelihood ratio
SC	sign correlator
GMSC	generalized memory-based sign correlator
pSC	prefiltered sign correlator
ISC	isotropic sign correlator
pISC	prefiltered isotropic sign correlator
vMyD	vector myriad detector
vGMD	vector geometric mean detector

the relative performance between detectors remains unaltered. This is discussed in detail in Section VI.

This paper is organized as follows. In Section II, we briefly explain concepts and the mathematical notation employed in our work. The LLR detector for αSGN(m) and the SC are presented in Section III. The LOD for αSGN(m) is derived in Section IV and its performance investigated. We present the GMSC and its variants in Section V. Simulation results in αSGN(m) and snapping shrimp noise are presented in Section VI-A, while detection performance in the underwater acoustical channel is investigated in Section VI-B. We wrap up by presenting the conclusions in Section VII.

II. Fundamental Concepts

A. NP Formulation

Under the NP framework of signal detection, our problem can be expressed as a binary hypotheses test [14]. Specifically, we need to determine whether the received samples $x_n \; \forall n \in \{1, 2, \ldots, N\}$ correspond to a signal and noise ($\mathcal{H}_1$) or a noise-only ($\mathcal{H}_0$) scenario. Mathematically, this is expressed as

$$\left.\begin{array}{l}\mathcal{H}_0 \; : \; x_n = w_n \\ \mathcal{H}_1 \; : \; x_n = \theta s_n + w_n\end{array}\right\} \forall n \in \{1, 2, \ldots, N\} \tag{1}$$

where $s_n, w_n \in \mathbb{R}$ and $\theta \in \mathbb{R}^+$ denote the transmitted signal, noise, and the signal strength, respectively. The transmitted signal is known as in the case of preamble detection for communication systems. One notes that the test is essentially a one-sided parameter test on θ, i.e., $\mathcal{H}_0 \; : \theta = 0$ and $\mathcal{H}_1 \; : \theta > 0$ [14]. One may alternatively express (1) in the convenient vector form

$$\begin{aligned}\mathcal{H}_0 \; &: \mathbf{x} = \mathbf{w} \\ \mathcal{H}_1 \; &: \mathbf{x} = \theta \mathbf{s} + \mathbf{w}\end{aligned} \tag{2}$$

where $\mathbf{x} = [x_1, x_2, \ldots, x_N]^\mathsf{T}$, $\mathbf{s} = [s_1, s_2, \ldots, s_N]^\mathsf{T}$, $\mathbf{w} = [w_1, w_2, \ldots, w_N]^\mathsf{T}$ and $[\cdot]^\mathsf{T}$ denotes the transpose. We denote the energy of the transmitted signal by $\mathcal{E}$, i.e., $\|\mathbf{s}\|^2 = \mathbf{s}^\mathsf{T}\mathbf{s} = \mathcal{E}$. The optimal detector for (1) or (2) is the LLR test. However, this requires *perfect* knowledge of the noise probability density function (PDF), $f_{\vec{W}}(\cdot)$, where $\vec{W}$ is the N-dimensional random vector with outcome $\mathbf{w}$ [14]. Moreover, the LLR detector requires an estimate of signal strength. The latter can be avoided by reverting to the LOD [5], [14].

Denoting the test statistic as $T(\mathbf{x})$, a detector decides on $\mathcal{H}_1$ if $T(\mathbf{x}) > \gamma$, and $\mathcal{H}_0$ otherwise where $\gamma \in \mathbb{R}$ is a predetermined threshold [14]. The probability of detection (P_D) is defined as the probability of $T(\mathbf{x}) > \gamma$ under $\mathcal{H}_1$, i.e., $P_\text{D} = P(T(\mathbf{x}) > \gamma; \mathcal{H}_1)$. Similarly, the probability of false alarm is given by $P_\text{FA} = P(T(\mathbf{x}) > \gamma; \mathcal{H}_0)$. In a typical setting, γ is determined for a certain P_FA. A good $T(\mathbf{x})$ is one that tries to maximize P_D for any given P_FA. Under this criterion, as per the NP Lemma, the LLR detector is optimal [14].

B. Snapping Shrimp Noise and WSαSN

Snapping shrimp noise exhibits both impulsiveness and memory. The latter property causes impulses to cluster together, thus making the process bursty [3], [6]. It is well known that the empirical amplitude distribution of snapping shrimp noise realizations are characterized well by the heavy-tailed SαS family [3], [5]. In [5], the Kolmogorov–Smirnov test was performed to test the goodness-of-fit for two snapping shrimp data sets sampled at 500 kHz. The test accepted an SαS distribution in either case with a significance level of 1%. Parameters of the accepted SαS distributions were estimated from the noise samples via McCulloch's method [15].

Univariate SαS distributions are characterized by two parameters, namely, the characteristic exponent $\alpha \in (0, 2]$ and the scale parameter $\delta \in \mathbb{R}^+$ [16]–[18]. Consequently, the distribution can be denoted by $\mathcal{S}(\alpha, \delta)$ [10]. SαS distributions are unimodal and generally heavy-tailed (algebraic-tailed). Moreover, the heaviness is completely determined by α. As $\alpha \to 2$, the tails become increasingly lighter, converging to a zero-mean Gaussian random variable with variance $2\delta^2$, i.e., $\mathcal{S}(2, \delta) \stackrel{d}{=} \mathcal{N}(0, 2\delta^2)$. The symbol $\stackrel{d}{=}$ denotes equality in distribution [16]. In snapping shrimp noise, typical estimates of α fall within the range $\alpha \geq 1.5$, with $\alpha = 1.5$ representing severe snapping shrimp noise [3], [5].

The WSαSN model has been used immensely in the literature to model snapping shrimp noise [5], [10], [19]. The term "white" implies that samples of WSαSN are IID SαS random variables. Consequently, the empirical amplitude distribution of its samples is SαS, which motivates its use to model snapping shrimp noise. However, the IID assumption does not allow WSαSN to characterize the memory between snapping shrimp noise samples. Therefore, detectors optimized for WSαSN cannot exploit the mutual information between the noise samples and thus fall within our definition of conventional robust detectors.

C. αSGN(m) Model

The αSGN(m) model was developed to characterize memory in snapping shrimp noise, while constraining the amplitude distribution to be SαS [6]. Recent works suggest substantial performance improvement in snapping shrimp noise when WSαSN-based detectors are replaced by ones optimized for αSGN(m) [11]–[13]. Further still, when αSGN(m) is tuned to snapping shrimp noise, several detectors offer similar performance in both the simulated and recorded noise scenarios [11], [13]. Such results validate the effectiveness of αSGN(m) in modeling snapping shrimp noise.

The αSGN(m) model is based on a sliding window framework and constrains any adjacent $m + 1$ samples to follow a (multivariate) α-sub-Gaussian (αSG) distribution [6]. The latter is essentially an elliptic heavy-tailed ($\alpha \neq 2$) SαS distribution [20]. More precisely, if $W_n \in \mathbb{R}$ denotes a sample of αSGN(m) at time index n and $\vec{W}_{n,m} = [W_{n-m}, W_{n-m+1}, \ldots, W_n]^\mathsf{T}$, then

$$\vec{W}_{n,m} = A_n^{1/2} \vec{G}_{n,m} \ \forall\, n \in \mathbb{Z}. \tag{3}$$

Here, A_n is a totally right-skewed real stable random *variable* and $\vec{G}_{n,m} = [G_{n-m}, G_{n-m+1}, \ldots, G_n]^\mathsf{T}$ is a zero-mean Gaussian random vector with the $(m+1)$ dimensional covariance matrix $\mathbf{R}_m = [r_{ij}]$, i.e., $\vec{G}_{n,m} \sim \mathcal{N}(\mathbf{0}, \mathbf{R}_m)$ [17], [20]. Both $\vec{W}_{n,m}$ and $\vec{G}_{n,m}$ are *real* random vectors of length $m + 1$. Moreover, A_n and $\vec{G}_{n,m}$ are independent of each other for all $n \in \mathbb{Z}$. As αSGN(m) is a stationary process, $\mathbf{R}_m$ does not change with time. Moreover, the sliding window framework constrains $\mathbf{R}_m$ to be a symmetric Toeplitz covariance matrix [6]. This allows constructing $\mathbf{R}_m$ in its entirety from any one of its rows or columns.

An SαS distribution is derived from the more general stable family of distributions [16], [17]. The latter is parametrized by two more parameters, namely, the skew $\beta \in [-1, 1]$ and location $\mu \in \mathbb{R}$. The corresponding distribution can be denoted by $\mathcal{S}(\alpha, \beta, \delta, \mu)$. An S$\alpha$S distribution is stable but with $\beta = \mu = 0$, i.e., $\mathcal{S}(\alpha, \delta) \stackrel{d}{=} \mathcal{S}(\alpha, 0, \delta, 0)$ [16], [17]. As all marginal distributions of an αSG random vector are αSG as well, W_n is an SαS random variable [20]. By employing $A_n \sim \mathcal{S}(\alpha/2, 1, 2(\cos(\pi\alpha/4))^{2/\alpha}, 0)$ and $r_{ii} = \delta^2 \ \forall\, i \in \{1, 2, \ldots, m\}$ in (3), we ensure that $W_n \sim \mathcal{S}(\alpha, \delta)$ [20]. We adhere to this parameterization in our manuscript. As $\alpha < 2$, αSGN(m) is clearly an impulsive process with amplitude distribution $\mathcal{S}(\alpha, \delta)$.

On a final note, we see that WSαSN is a special instance of αSGN(m), which arises when $m = 0$. In this instance, (3) simplifies to

$$W_n = A_n^{1/2} G_n \ \forall\, n \in \mathbb{Z} \tag{4}$$

where A_n and G_n are independent random variables. Moreover, both A_n and G_n are independent of A_t and G_t for $t \neq n$. We also note that G_n is essentially a white Gaussian noise (WGN) process in this scenario.

D. On Regression and Spectral Form

Though we have commented on its stationarity, we note that αSGN(m) is also a Markov process of order m. This observation stems directly from (3) and is a consequence of the sliding window framework [6], [21]. Mathematically, let w_n and $\mathbf{w}_{n,m} = [w_{n-m}, w_{n-m+1}, \ldots, w_n]^\mathsf{T}$ denote outcomes of W_n and $\vec{W}_{n,m}$, respectively. Then the distribution of W_n conditional on all previous samples, i.e., up until w_{n-1}, is equivalent to that of the conditional random variable $W_n | \vec{W}_{n-1,m-1} = \mathbf{w}_{n-1,m-1}$. Similarly, from (3), we note that the underlying Gaussian process is also stationary and Markov. In fact, G_n are samples of a Gaussian m-order autoregressive (AR(m)) process whose coefficients can be completely determined from $\mathbf{R}_m$.

More precisely, we can express $\mathbf{R}_m$ in the block matrix form

$$\mathbf{R}_m = \begin{bmatrix} \mathbf{R}_{m-1} & \mathbf{r}_m \\ \mathbf{r}_m^\mathsf{T} & \delta^2 \end{bmatrix} \tag{5}$$

where $\mathbf{r}_m = [r_1, r_2, \ldots, r_m]^\mathsf{T}$. This leads to the expression

$$\begin{aligned} G_n &= \mathbf{r}_m^\mathsf{T} \mathbf{R}_{m-1}^{-1} \vec{G}_{n-1,m-1} + \sqrt{\kappa} Z_n \\ &= \sum_{k=1}^{m} \psi_k G_{n-k} + \sqrt{\kappa} Z_n \end{aligned} \tag{6}$$

where $Z_n \sim \mathcal{N}(0,1)$ are IID random variables for all $n \in \mathbb{Z}$ and $\kappa = \delta^2 - \mathbf{r}_m^\mathsf{T} \mathbf{R}_{m-1}^{-1} \mathbf{r}_m = \det \mathbf{R}_m / \det \mathbf{R}_{m-1}$ is the Schur's complement of $\mathbf{R}_{m-1}$ [21, eq. (20)]. As $\mathbf{R}_m$ (and therefore $\mathbf{R}_{m-1}$) is positive semidefinite, $\kappa \in \mathbb{R}^+$. Moreover, on defining $\boldsymbol{\psi} = [\psi_1, \psi_2, \ldots, \psi_m]^\mathsf{T}$, we have

$$\boldsymbol{\psi} = \mathbf{r}_m^\mathsf{T} \mathbf{R}_{m-1}^{-1} \mathbf{J}_m$$

where $\mathbf{J}_m$ is the $m \times m$ a reversal matrix, i.e., it has unit elements on its antidiagonal and is zero elsewhere.

In the spectral domain, densities evaluated from αSGN(m) realizations exhibit the same shape as the power spectral density (PSD) of the underlying Gaussian process [11]. Note, that the PSD of αSGN(m) does not exist as second-order moments of SαS random variables ($\alpha \neq 2$) are infinite [17], [18]. However, analogous to the relationship between scale and variance in $\mathcal{S}(2,\delta) \stackrel{d}{=} \mathcal{N}(0, 2\delta^2)$, the PSD of G_n can be defined as the pseudoPSD (PPSD) of the αSGN(m) process. By denoting the one-sided PSD of G_n by $P_g(f)$, we have from [11, eq. (34)] [22]

$$P_g(f) = \frac{2\kappa}{|1 - \sum_{k=1}^{m} \psi_k e^{-j2\pi k f}|^2}, \qquad \text{for } 0 \le f < 1/2. \tag{7}$$

Note that our definition of the PPSD is independent of α and thus exists for all $\alpha \neq 2$.

For the special case of $\mathbf{R}_m = \delta^2 \mathbf{I}_{m+1}$, where $\mathbf{I}_m$ is the size m identity matrix, G_n is a WGN process. Consequently, $\boldsymbol{\psi} = \mathbf{0}$ and $P_g(f) = 2\kappa$. From (3), $\mathbf{R}_m = \delta^2 \mathbf{I}_{m+1}$ implies that $\vec{W}_{n,m}$ is an isotropic αSG random vector and therefore its elements are *not* independent [20]. Thus, the PPSD is essentially flat but the αSGN(m) samples still exhibit memory due to A_n. We term this process as isotropic αSGN(m). On the other hand, to ensure independence, one must invoke $m = 0$, which limits the sliding window to a single sample and results in WSαSN. Note that both isotropic αSGN(m) and WSαSN have flat (white) PPSDs. Yet, in the literature, the term "white" implies IID samples for WSαSN [10], [19]. As this does not extend to the former, one should be careful when treating these processes.

To make good use of the αSGN(m) model, it is important that we tune its parameters robustly from snapping shrimp noise [6], [7]. For a given m, the parameters that need to be estimated are α and $r_{1j} \forall\, j \in \{1, 2, \ldots, m+1\}$. Therefore, a total of $m+2$ parameters need to be estimated. It may be convenient to separate the scale from $\mathbf{R}_m$ and consider the normalized covariance matrix with unit diagonal entries $\acute{\mathbf{R}}_m = \mathbf{R}_m / \delta^2$, which from

TABLE II
r_{1j}/δ^2 FROM SNAPPING SHRIMP NOISE SAMPLED AT 180 kHz

j	$\hat{r}_{1j}/\hat{\delta}^2$
1	1.000
2	0.662
3	0.308
4	0.182
5	0.045
6	0.029
7	0.018
8	– 0.038
9	– 0.103

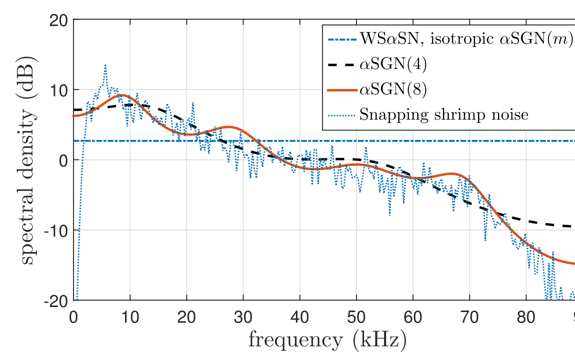

Fig. 1. Comparison of spectral densities of αSGN(m) and snapping shrimp noise.

(5) has the block matrix form

$$\acute{\mathbf{R}}_m = \begin{bmatrix} \acute{\mathbf{R}}_{m-1} & \mathbf{r}_m/\delta^2 \\ \mathbf{r}_m^\mathsf{T}/\delta^2 & 1 \end{bmatrix}. \tag{8}$$

We can equivalently state that αSGN(m) is parameterized by α, δ, and $r_{1j}/\delta^2 \;\forall\, j \in \{2, 3, \ldots, m+1\}$. In our work, we adopt the estimation scheme outlined in [6], which is based on the approach initially employed in [23]. The method initially fits a SαS PDF to the empirical amplitude density function of a snapping shrimp noise realization. This is accomplished by evaluating α and δ by the method of ML under the assumption of WSαSN. The elements $r_{1j} \forall\, j \in \{2, 3, \ldots, m+1\}$ are then subsequently estimated by a covariation-based method that evaluates each r_{1j} separately. Each estimate is independent of the model order. Therefore, the estimation scheme assumes $\mathbf{R}_{\acute{m}}$ to be the top-left $\acute{m} \times \acute{m}$ submatrix of $\mathbf{R}_m$ for any $\acute{m} < m$.

We consider a 1300-s-long snapping shrimp noise data set sampled at 180 kHz and bandpass filtered within the range 2–75 kHz. The data are initially split into blocks of 10^6 samples ($\sim$5.56 s long). For each block, the parameters of the αSGN(m) model are estimated via the scheme in [6]. By averaging the estimates over all blocks we get the overall estimate of the noise data set. A maximum order of $m = 8$ is considered. The estimated parameters are $\hat{\alpha} = 1.57$ and $\hat{\delta} = 12.92$, with the normalized elements $\hat{r}_{1j}/\hat{\delta}^2 \;\forall\, j \in \{1, 2, \ldots, 9\}$ given in Table II. In Fig. 1, we present the PSD of the first 10^6 samples of the noise data. The well-known nonparametric Welch method is applied to get this result [24]. Also plotted are the PPSDs [from (7)] for αSGN(4) and αSGN(8). For comparison, we also plot the PPSD for

WSαSN, which essentially is the same for isotropic αSGN(m) for all $m > 0$. In both of these cases, only α and δ need to be estimated. For all models, the area under the PPSD curve is $\hat{\delta}^2$. As the Welch method is not robust to impulses, the snapping shrimp noise curve is normalized such that the area under it is equal to $\hat{\delta}^2$. Clearly, of all the PPSDs shown in Fig. 1, the αSGN(m) curves for $m = 4$ and $m = 8$ offer better proximity to the empirical PSD. Order selection is based on observations highlighted in our previous works [7], [11], [21]. The $m = 4$ case results from visually tracking elliptical structures in delay scatter plots of snapping shrimp noise samples at 180 kHz [6], [11], while $m = 8$ stems from temporal analysis of its impulsive events [7].

Now that we have sufficiently described the αSGN(m) model, we go back to the NP formulation discussed in Section II-A. The samples $w_n \; \forall \; n \in \{1, 2, \ldots, N\}$ are considered to be outcomes of αSGN(m). We briefly review two robust detectors next, namely, the SC and the LLR detector for αSGN(m). These will be used to benchmark performance for our proposed schemes later on.

III. Revisiting Select Robust Detectors in Snapping Shrimp Noise

A. LLR Detector for αSGN(m)

The LLR detector for αSGN(m) was derived in [11] and was shown to outperform several conventional robust detectors in snapping shrimp noise. The LLR test statistic is given by

$$T(\mathbf{x}) = \log \frac{f_{\vec{W}}(\mathbf{x} - \theta \mathbf{s})}{f_{\vec{W}}(\mathbf{x})}. \tag{9}$$

The joint-PDF $f_{\vec{W}}(\cdot)$ can be expressed in terms of its conditional PDFs [25, p. 253]

$$f_{\vec{W}}(\mathbf{w}) = \prod_{n=1}^{N} f_{W_n|\vec{W}_{n-1}}(w_n|\mathbf{w}_{n-1})$$

where $\vec{W}_n = [W_1, W_2, \ldots, W_n]^\mathsf{T}$ is an n-dimensional random vector and $\mathbf{w}_n = [w_1, w_2, \ldots, w_n]^\mathsf{T}$ its outcome. As αSGN(m) is stationary and Markov, $f_{\vec{W}}(\cdot)$ can be further expressed as [11, eqs. (19)]

$$\begin{aligned} f_{\vec{W}}(\mathbf{w}) &= f_{\vec{W}_m}(\mathbf{w}_m) \prod_{n=m+1}^{N} f_{W_{m+1}|\vec{W}_m}(w_n|\mathbf{w}_{n-1,m-1}) && (10) \\ &= f_{\vec{W}_m}(\mathbf{w}_m) \prod_{n=m+1}^{N} \frac{f_{\vec{W}_{m+1}}(\mathbf{w}_{n,m})}{f_{\vec{W}_m}(\mathbf{w}_{n-1,m-1})}. && (11) \end{aligned}$$

The PDFs $f_{\vec{W}_{m+1}}(\cdot)$ and $f_{\vec{W}_m}(\cdot)$ are essentially αSG PDFs with covariance matrices $\mathbf{R}_m$ and $\mathbf{R}_{m-1}$, respectively. One notes that (9) requires *robust* estimates of θ and the parameters of the αSGN(m) process before it can be employed.

B. Sign Correlator

The SC has been employed successfully in the literature to mitigate snapping shrimp noise [5], [26]. The detector is particularly attractive as it is nonparametric, extremely simple to implement and performs at par with parametric robust detectors in snapping shrimp noise [5]. The SC can be derived from the LOD for a noise process with IID samples. The latter is optimal for $\theta = 0$ and can be expressed as $T(\mathbf{x}) = \sum_{n=1}^{N} -f'_W(x_n)/f_W(x_n)s_n$, where $f_W(\cdot)$ is the univariate PDF of a single noise sample and $f'_W(\cdot)$ is its first-order derivative. We note that the LOD is obtained from a linear correlation between the sampled signal s_n and the nonlinear function

$$\ell(x_n) = -f'_W(x_n)/f_W(x_n). \tag{12}$$

$\ell(\cdot)$ can be replaced by a more general easy-to-implement nonlinear function $g(\cdot)$ to get

$$T(\mathbf{x}) = \sum_{n=1}^{N} g(x_n)s_n. \tag{13}$$

The motivation for using a customized $g(\cdot)$ instead of the original nonlinearity is to do away with model mismatch. Moreover, $g(\cdot)$ can be of a simpler form and yet still offer good (or even better) performance in practice. The SC is a special case of this family and is given by

$$T(\mathbf{x}) = \sum_{n=1}^{N} \mathtt{sign}(x_n)s_n \tag{14}$$

where $g(x) = \mathtt{sign}(x)$ is the sign function, i.e.,

$$\mathtt{sign}(x) = \begin{cases} 1, & \text{if } x > 0 \\ 0, & \text{if } x = 0 \\ -1, & \text{if } x < 0. \end{cases}$$

As $\mathtt{sign}(\cdot)$ is a bounded function, we note that the SC is a robust detector. Moreover, the SC does not take memory of the noise process into account and is therefore robust in the conventional sense. Note that though the LOD is independent of θ, it is still parametric and requires $f_W(\cdot)$, i.e., estimates of α and δ. The SC removes this dependence completely and is thus nonparametric. Due to its simplicity and excellent performance in snapping shrimp noise [5], the SC is an attractive prospect for implementation in practical systems.

C. Other Robust Detectors

In [11], besides deriving the LLR detector for αSGN(m), we proposed two new detectors, namely the vector myriad detector (vMyD) and the vector geometric mean detector (vGMD). The proposed schemes are based on constructs found in generalized ML estimation theory. More precisely, $f_{\vec{W}_m}(\cdot)$ and $f_{\vec{W}_{m+1}}(\cdot)$ in (11) are replaced by more general functions $\rho_m(\cdot)$ and $\rho_{m+1}(\cdot)$, respectively, where $\rho_m(\cdot),\; \rho_{m+1}(\cdot) \in \mathbb{R}^+$. The motivation for doing so stems from the fact that SαS PDFs do not exist in closed form. Ideally, the elemental functions should offer close approximations to the corresponding joint-PDFs. For the case of the vMyD, $\rho_m(\cdot)$ and $\rho_{m+1}(\cdot)$ are based on the myriad cost function [9], whereas the vGMD is a special case of the vMyD. Both schemes were shown to perform at par with the LLR detector [11]. Further still, the vGMD was shown to be a semiparametric detector, requiring no information about α and δ whatsoever. In our work, we do not consider vMyD or vGMD because even though they offer performance comparable to the LLR detector at reduced computational complexity, their complexity is not small enough to be realized in practical communication systems. The latter is discussed further in Section IV-B. For more information, [11] offers a comprehensive treatment of the vMyD and vGMD and also compares them to their conventional counterparts, namely, the MyD and the GMD, respectively.

IV. Locally Optimal Detection in αSGN(m)

One way to reduce the dependency of (9) on its parameters is to consider locally optimal detection [14]. As highlighted in Section III-B, the latter is attractive in the sense that it does not require an estimate of θ. The detectors proposed later on are derived from the LOD for αSGN(m) and inherently include this property. We therefore devote this section to the derivation and analysis of locally optimal detection in αSGN(m).

A. Derivation, Results, and Analysis

Under the NP framework in (2), the LOD for αSGN(m) (which from here on we just term as the LOD) is given by [27, eq. (3)]

$$T(\mathbf{x}) = \frac{\frac{\partial}{\partial\theta} f_{\vec{W}}(\mathbf{x} - \theta\mathbf{s})|_{\theta=0}}{f_{\vec{W}}(\mathbf{x})}. \quad (15)$$

On substituting $\mathbf{u} = \mathbf{x} - \theta\mathbf{s}$ and invoking the chain rule, i.e., $\partial f_{\vec{W}}(\mathbf{x} - \theta\mathbf{s})/\partial\theta = \left(\partial f_{\vec{W}}(\mathbf{u})/\partial\mathbf{u}\right)^{\mathsf{T}}\partial\mathbf{u}/\partial\theta = -\left(\partial f_{\vec{W}}(\mathbf{u})/\partial\mathbf{u}\right)^{\mathsf{T}}\mathbf{s}$, we get

$$\begin{aligned} T(\mathbf{x}) &= -\frac{\left(\frac{\partial}{\partial\mathbf{x}} f_{\vec{W}}(\mathbf{x})\right)^{\mathsf{T}}}{f_{\vec{W}}(\mathbf{x})}\mathbf{s} \\ &= \sum_{n=1}^{N} \underbrace{\left(-\frac{\frac{\partial}{\partial x_n} f_{\vec{W}}(\mathbf{x})}{f_{\vec{W}}(\mathbf{x})}\right)}_{\ell_n(\mathbf{x})} s_n. \end{aligned} \quad (16)$$

Though (12) and (16) may seem similar at first glance, we note that $\ell_n(\mathbf{x})$ denotes a family of N functions indexed by $n \in \{1, 2, \ldots, N\}$. Moreover, they can only be evaluated once $\mathbf{x}$ is *completely* acquired. This stands in stark contrast to (12), where $\ell(x_n)$ requires only the current sample, thus allowing it to be evaluated over time. However, one can take advantage of the form in (11) to simplify (16). To allow concise notation, we drop the subscripts of each αSG PDF in (11) and let the argument highlight its dimensionality. The resulting $\ell_n(\mathbf{x})$ is

$$\ell_n(\mathbf{x}) = \begin{cases} -\sum\limits_{i=m+1}^{\min(n+m,N)} \frac{\frac{\partial}{\partial x_n} f(\mathbf{x}_{i,m})}{f(\mathbf{x}_{i,m})} + \sum\limits_{i=m+2}^{\min(n+m,N)} \frac{\frac{\partial}{\partial x_n} f(\mathbf{x}_{i-1,m-1})}{f(\mathbf{x}_{i-1,m-1})} & n \le m \\ -\sum\limits_{i=n}^{\min(n+m,N)} \frac{\frac{\partial}{\partial x_n} f(\mathbf{x}_{i,m})}{f(\mathbf{x}_{i,m})} + \sum\limits_{i=n+1}^{\min(n+m,N)} \frac{\frac{\partial}{\partial x_n} f(\mathbf{x}_{i-1,m-1})}{f(\mathbf{x}_{i-1,m-1})} & n > m. \end{cases} \quad (17)$$

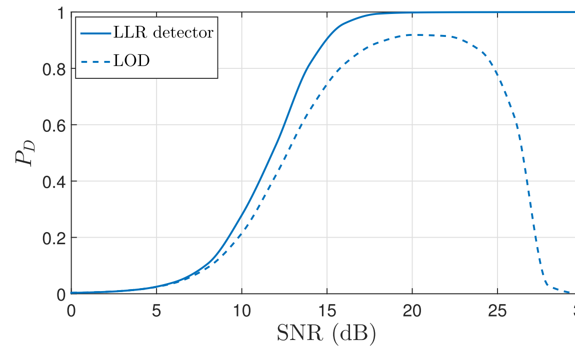

Fig. 2. Comparison of the LOD and LLR detector for $N = 100$, $\alpha = 1.5$, and $P_{\mathrm{FA}} = 10^{-4}$.

The reader is directed toward Appendix A for a complete derivation. For brevity, one can express (17) equivalently as

$$\begin{aligned} \ell_n(\mathbf{x}) = &-\sum_{i=\max(m+1,n)}^{\min(n+m,N)} \frac{\frac{\partial}{\partial x_n} f(\mathbf{x}_{i,m})}{f(\mathbf{x}_{i,m})} \\ &+ \sum_{i=\max(m+2,n+1)}^{\min(n+m,N)} \frac{\frac{\partial}{\partial x_n} f(\mathbf{x}_{i-1,m-1})}{f(\mathbf{x}_{i-1,m-1})}. \end{aligned} \quad (18)$$

The expressions in (17) and (18) assume $N > m$. This case is of interest as m is small (refer to Fig. 1) and N is typically set to a large value. Moreover, for $N \le m$, the case is trivial as $f(\mathbf{x})$ is itself αSG and (16) highlights its simplified form.

Before we investigate the LOD's performance, a suitable SNR measure needs to be defined. Based on our previous work [11], [13], we employ SNR $= \mathcal{E}\theta^2/(2\delta^2)$ in our simulations. Note that our definition of SNR does not depend on the in-band noise power but on the *average* noise power achieved by integrating the PSD/PPSD. A detailed explanation for this choice of SNR is offered in [11, p. 9].

In Fig. 2, we plot P_{D} against SNR for the LOD and LLR detector in αSGN(4) for $\alpha = 1.5$. We employ $P_{\mathrm{FA}} = 10^{-4}$, $N = 100$, and construct $\mathbf{R}_4$ from Table II. Both detectors are clairvoyant. The noise model for this example characterizes severe snapping shrimp noise sampled at 180 kHz. We employ a linear chirp of bandwidth 18 kHz centered at 25 kHz as the transmitted signal. One can clearly see that the LOD's performance approaches the LLR curve at low SNR. However, the performance tends to deviate with increasing SNR. In fact, the LOD breaks down completely at high SNR. To understand why, we plot a realization of x_n and $\ell_n(\mathbf{x})$ for $N = 1000$ in Fig. 3. We consider $\mathcal{H}_0$ in this example, thus x_n are samples of αSGN(4) and the LOD is optimal ($\theta = 0$). We observe that x_n consists of a large burst and $\ell_n(\mathbf{x})$ severely penalizes the samples within. Though this is near-optimal at low SNR, it is clearly problematic at high SNR. In the latter scenario, any large sample is penalized, irrespective of it being part of a burst or the desired signal. Though performance can be improved by increasing N [14], it comes with added computational cost.

We show that one can modify (18) to achieve better detection performance at medium-to-high SNR. To do so, we need to express (18) in a better representative form. From (18), we note that

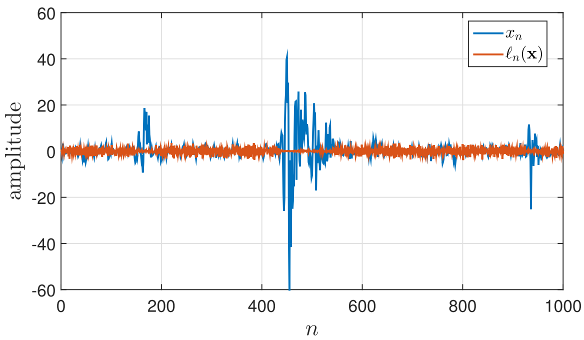

Fig. 3. A realization of x_n and $\ell_n(\mathbf{x})$ in αSGN(4) under $\mathcal{H}_0$.

the LOD depends on the functions $\partial/\partial x_n f(\mathbf{x}_{i,m})/f(\mathbf{x}_{i,m})$ and $\partial/\partial x_n f(\mathbf{x}_{i-1,m-1})/f(\mathbf{x}_{i-1,m-1})$. As both expressions have similar constructs, we focus on the former as results can be trivially extended to the latter.

The αSG PDF $f(\mathbf{z})$, for some $\mathbf{z} \in \mathbb{R}^{m+1}$, can be expressed as [21, eq. (8)]

$$f(\mathbf{z}) = \frac{\Gamma(\frac{m+1}{2})}{2\pi^{(m+1)/2}} v(\|\mathbf{R}_m^{-1/2}\mathbf{z}\|; \alpha, m+1) \tag{19}$$

where $\Gamma(\cdot)$ is the gamma function and $v(r;\alpha,m+1)$ is a function parameterized by α and m. Moreover, $\mathbf{R}_m^{-1/2}$ stems from the Cholesky decomposition of $\mathbf{R}_m^{-1}$, i.e., $\mathbf{R}_m^{-1} = (\mathbf{R}_m^{-1/2})^\mathsf{T}\mathbf{R}_m^{-1/2}$. Let $\mathbf{d}_k^{(m)}$ denote the k^{th} column of $\mathbf{R}_m^{-1}$, i.e., $\mathbf{R}_m^{-1} = [\mathbf{d}_1^{(m)}, \mathbf{d}_2^{(m)}, \ldots, \mathbf{d}_{m+1}^{(m)}]$. Then, from (19) we have

$$\begin{aligned}\frac{\frac{\partial}{\partial z_k} f(\mathbf{z})}{f(\mathbf{z})} &= \frac{\frac{\partial}{\partial z_k} v(\|\mathbf{R}_m^{-1/2}\mathbf{z}\|;\alpha,m+1)}{v(\|\mathbf{R}_m^{-1/2}\mathbf{z}\|;\alpha,m+1)} \\ &= \underbrace{\frac{\mathbf{z}^\mathsf{T}\mathbf{d}_k^{(m)}}{\|\mathbf{R}_m^{-1/2}\mathbf{z}\|}}_{\zeta_1(\mathbf{z})} \underbrace{\left.\frac{\frac{\partial}{\partial r} v(r;\alpha,m+1)}{v(r;\alpha,m+1)}\right|_{r=\|\mathbf{R}_m^{-1/2}\mathbf{z}\|}}_{\zeta_2(\mathbf{z})}\end{aligned} \tag{20}$$

for $k \in \{1,2,\ldots,m+1\}$. Note that $\partial/\partial x_n f(\mathbf{x}_{i,m})/f(\mathbf{x}_{i,m})$ for $\max(m+1,n) \le i \le \min(n+m,N)$ is obtained from (20) by replacing k and $\mathbf{z}$ with $n-i+m+1$ and $\mathbf{x}_{i,m}$, respectively. As the regime of interest in Fig. 3 corresponds to large x_n, we briefly investigate what happens to (20) in such a scenario. This is accomplished by employing $\mathbf{z} = c\bar{\mathbf{z}}$, where $c \in \mathbb{R}^+$ is an arbitrary scale, and analyzing the impact of large c on $\zeta_1(\mathbf{z})$ and $\zeta_2(\mathbf{z})$.

From [21], we know that the tails of $v(r;\alpha,m+1)$ decay as a power law. This results in the limiting form

$$\lim_{r\to\infty} |r|^{\alpha+m+1} v(r;\alpha,m+1) = \alpha k(\alpha,m+1) \tag{21}$$

where $k(\cdot)$ depends only on α and m. Then, for sufficiently large c, we have the approximation

$$\zeta_2(\mathbf{z}) \approx -\frac{\alpha+m+1}{\|\mathbf{R}_m^{-1/2}\mathbf{z}\|} = -\frac{\alpha+m+1}{c\|\mathbf{R}_m^{-1/2}\bar{\mathbf{z}}\|}. \tag{22}$$

Clearly, $\zeta_2(\mathbf{z})$ is inversely proportional to c and tends to zero when $c \to \infty$. On the other hand, $\zeta_1(\mathbf{z})$ is invariant to scale, i.e.,

$$\zeta_1(\mathbf{z}) = \frac{(c\bar{\mathbf{z}})^\mathsf{T}\mathbf{d}_k^{(m)}}{\|\mathbf{R}_m^{-1/2}(c\bar{\mathbf{z}})\|} = \frac{\bar{\mathbf{z}}^\mathsf{T}\mathbf{d}_k^{(m)}}{\|\mathbf{R}_m^{-1/2}\bar{\mathbf{z}}\|} \qquad \forall\, c \in \mathbb{R}^+ \tag{23}$$

and is also bounded, i.e.,

$$|\zeta_1(\mathbf{z})| \le \sqrt{\frac{\lambda_{\max}(\mathbf{R}_m^{-1})}{\lambda_{\min}(\mathbf{R}_m^{-1})}} \tag{24}$$

where $\lambda_{\min}(\cdot)$ and $\lambda_{\max}(\cdot)$ output the minimum and maximum eigenvalues of their matrix arguments, respectively. The reader is directed toward Appendix B for a proof.

The above insights (for sufficiently large c) can be applied to (18). On substituting (22) in (20), we have the closed-form approximation

$$\frac{\frac{\partial}{\partial z_k} f(\mathbf{z})}{f(\mathbf{z})} \approx -(\alpha+m+1)\frac{\mathbf{z}^\mathsf{T}\mathbf{d}_k^{(m)}}{\|\mathbf{R}_m^{-1/2}\mathbf{z}\|^2}. \tag{25}$$

By appropriately updating the indices, this can then be substituted in (18) and normalized by $\alpha+m$ to get

$$\begin{aligned}\ell_n(\mathbf{x}) \approx \eta \sum_{i=\max(m+1,n)}^{\min(n+m,N)} \frac{\mathbf{x}_{i,m}^\mathsf{T}\mathbf{d}_{n-i+m+1}^{(m)}}{\|\mathbf{R}_m^{-1/2}\mathbf{x}_{i,m}\|^2} \\ - \sum_{i=\max(m+2,n+1)}^{\min(n+m,N)} \frac{\mathbf{x}_{i-1,m-1}^\mathsf{T}\mathbf{d}_{n-i+m+1}^{(m-1)}}{\|\mathbf{R}_{m-1}^{-1/2}\mathbf{x}_{i-1,m-1}\|^2}\end{aligned} \tag{26}$$

where $\eta = \alpha+m+1/\alpha+m$. Note that the normalization in (26) does not influence the performance of (16) if the detection threshold is scaled accordingly. From (26), if the elements within $\mathbf{x}_{i,m}$ correspond to a burst or a strong signal, then the corresponding summand (and that of $\mathbf{x}_{i-1,m-1}$) are close to zero. If the burst starts at x_n and spans more than $m+1$ consecutive samples, then $\ell_n(\mathbf{x}) \approx 0$, as *all* summands in (26) [and thus (18)] are effectively zero. From (23), the excessive penalty in (26) can be clearly avoided by relaxing the term in its denominator.

Analogous to (13), we replace $\ell_n(\cdot)$ in (16) by the more general function $g_n(\cdot)$ to get

$$T(\mathbf{x}) = \sum_{n=1}^{N} g_n(\mathbf{x}) s_n. \tag{27}$$

Our approach is to employ the limiting form in (26) as $g_n(\mathbf{x})$, but with $\|\mathbf{R}_m^{-1/2}\mathbf{z}\|^2$ replaced in the denominator by $\|\mathbf{R}_m^{-1/2}\mathbf{z}\|$. By doing so, we are left with a scale invariant term that is also bounded. These properties are highlighted by (23) and (24), respectively. This results in

$$\begin{aligned}g_n(\mathbf{x}) = \eta \sum_{i=\max(m+1,n)}^{\min(n+m,N)} \frac{\mathbf{x}_{i,m}^\mathsf{T}\mathbf{d}_{n-i+m+1}^{(m)}}{\|\mathbf{R}_m^{-1/2}\mathbf{x}_{i,m}\|} \\ - \sum_{i=\max(m+2,n+1)}^{\min(n+m,N)} \frac{\mathbf{x}_{i-1,m-1}^\mathsf{T}\mathbf{d}_{n-i+m+1}^{(m-1)}}{\|\mathbf{R}_{m-1}^{-1/2}\mathbf{x}_{i-1,m-1}\|}.\end{aligned} \tag{28}$$

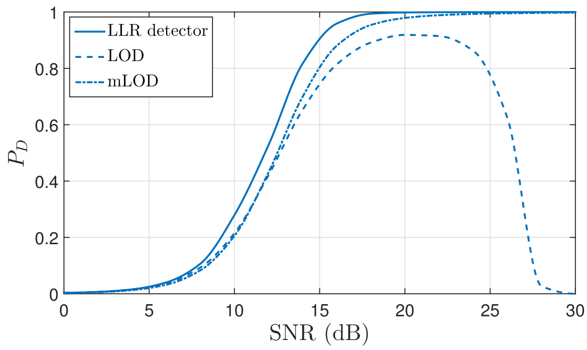

Fig. 4. Comparison of the LOD, LLR, and mLOD for $N = 100$, $\alpha = 1.5$, and $P_{\text{FA}} = 10^{-4}$.

From (24), we note that (28) is bounded by

$$|g_n(\mathbf{x})| \le \eta(m+1)\sqrt{\frac{\lambda_{\max}(\mathbf{R}_m^{-1})}{\lambda_{\min}(\mathbf{R}_m^{-1})}} + m\sqrt{\frac{\lambda_{\max}(\mathbf{R}_{m-1}^{-1})}{\lambda_{\min}(\mathbf{R}_{m-1}^{-1})}} \quad (29)$$

for all $n \in \{1, 2, \ldots, N\}$. Therefore, (28) guarantees (27) to be a robust statistic, which we term as the modified LOD (mLOD). Moreover, the latter has a closed form and also takes the memory of αSGN(m) into account.

We plot the detection performance of the mLOD in Fig. 4. The simulation setting is the same as that for Fig. 2. For comparison, the LLR and LOD performance curves are also redrawn here. As expected, the mLOD clearly outperforms the LOD at intermediate-to-high SNR. Moreover, it performs almost at par with the LOD at low SNR.

On a final note, we can extend the argument in (23) to (28), i.e., $g_n(\mathbf{x}) = g_n(\bar{\mathbf{x}})$ for any $c \in \mathbb{R}^+$ where $\mathbf{x} = c\bar{\mathbf{x}}$. Moreover, as scaling $T(\mathbf{x})$ does not alter detection performance if the threshold is scaled accordingly, the mLOD is independent of δ as well. Consequently, from (8), one can substitute $\mathbf{d}_k^{(m)}$ and $\mathbf{R}_m^{-1}$ in (28) by the scale-normalized forms $\acute{\mathbf{d}}_k^{(m)} = \mathbf{d}_k^{(m)}\delta^2$ and $\acute{\mathbf{R}}_m^{-1} = \mathbf{R}_m^{-1}\delta^2$, respectively. The same can be done to the corresponding bound in (29), which remains unchanged.

B. Computational Complexity

We now discuss the computational complexity of the detectors for each received passband sample. This would be used in applications such as preamble detection for communication. As linear baseband conversion is very suboptimal in impulsive noise [10], [28], it is desirable to implement the detectors in passband. Our formulation takes this into account as snapping shrimp noise [and thus αSGN(m)] is a passband noise process. However, such implementations are problematic as computations need to be performed at rates proportional to the passband sampling frequency. Simple schemes such as the SC are therefore attractive in this regard. From (14), for a newly acquired sample (designated as x_N) the SC requires one comparison to determine the sign, followed by N multiplication and $N-1$ addition operations. This results in a cost of $\mathcal{O}(N)$.

In general, a detector of the form in (27) offers linear complexity in N. Moreover $g_n(\mathbf{x})$ needs to be updated too. As αSGN(m) is Markov, the mLOD's computations are significantly reduced. To be precise, for every newly received sample x_N, only $g_n(\mathbf{x}) \, \forall \, n \in \{N-m, N-m+1, \ldots, N\}$ needs to be updated. In turn, from (28), this requires evaluating $\|\mathbf{R}_m^{-1/2}\mathbf{x}_{N,m}\|$, $\|\mathbf{R}_{m-1}^{-1/2}\mathbf{x}_{N-1,m-1}\|$, $\mathbf{x}_{N,m}^{\mathsf{T}}\mathbf{R}_m^{-1}$, and $\mathbf{x}_{N-1,m-1}^{\mathsf{T}}\mathbf{R}_{m-1}^{-1}$. Therefore, updating $g_n(\mathbf{x})$ is quadratic in m and results in an overall complexity of $\mathcal{O}(m^2+N)$ per received sample for the mLOD.

For the LLR detector, the computational cost is significantly larger. Not including the cost of computing αSG PDFs, the LLR detector's complexity is $\mathcal{O}(m^2N)$ for every received sample. To see why, we first note that $\|\mathbf{R}_m^{-1/2}\mathbf{z}\|$ in (19) requires $\mathcal{O}(m^2)$ computations. On substituting (19) in (11), we see that the denominator in (9) can be aggregated over time. More precisely, for every received sample x_N, only $f(\mathbf{x}_{N,m})$ and $f(\mathbf{x}_{N-1,m-1})$ need to be evaluated which results in $\mathcal{O}(m^2)$ complexity. On the other hand, $f_{\vec{W}}(\mathbf{x}-\theta\mathbf{s})$ in (9) requires computing $\mathbf{x}-\theta\mathbf{s}$, which runs in $\mathcal{O}(N)$ time. Furthermore, all $2(N-m)+1$ αSG PDFs in (11) need to be evaluated. As each PDF's argument computes in $\mathcal{O}(m^2)$ time and $N \gg m$, $f_{\vec{W}}(\mathbf{x}-\theta\mathbf{s})$ is of $\mathcal{O}(m^2N)$ complexity. This results in an overall runtime of $\mathcal{O}(m^2N)$ to just compute the arguments of the LLR detector. For our range of interest, $1.5 \le \alpha < 2$, the computational complexity is even greater as αSG PDFs do not exist in closed form [17], [18]. Consequently, elemental PDFs in (11) need to be numerically evaluated at rates on the order of the passband sampling frequency. Though this can be avoided by employing closed-form approximations such as the near-optimal vMyD and vGMD [11], they nevertheless still compute in $\mathcal{O}(m^2N)$ time. Moreover, the LLR detector or its closed-form variants require robust estimates of the model's parameters and θ. The former set can be computed offline and averaged over several noise realizations [11]. In such a case, the detector is expected to perform well on an average. However, θ still needs to be estimated in real time. All of the aforementioned issues make implementing the LLR detector and its variants very challenging in practice.

V. Locally Optimal Inspired Detectors in αSGN(m)

The mLOD offers near-optimal performance in αSGN(m) and its form inspires the detectors proposed in this section. Our objective is to come up with low-complexity schemes that are dependent on a smaller parameter space with respect to the NP detector, yet still offer robust performance in snapping shrimp noise. The resulting detectors exploit memory and perform much better than the SC with only a little computational overhead.

A. Generalized Memory-Based Sign Correlator

As highlighted in Section III-C, the vGMD is essentially a closed-form approximation of the LLR detector in αSGN(m). The vGMD is near-optimal but requires no knowledge of α whatsoever. Inspired by this and the fact that $\eta > 1$ in (28), we propose the nonlinearity

$$g_n(\mathbf{x}) = \sum_{i=\max(m+1,n)}^{\min(n+m,N)} \frac{\mathbf{x}_{i,m}^{\mathsf{T}}\acute{\mathbf{d}}_{n-i+m+1}^{(m)}}{\|\acute{\mathbf{R}}_m^{-1/2}\mathbf{x}_{i,m}\|}. \quad (30)$$

We note that (30) is merely (28) but with $\eta \to \infty$. Clearly, (30) is no longer dependent on α. We term the corresponding detector as the GMSC due to its simplicity and the fact that $g_n(\mathbf{x}) = \mathtt{sign}(x_n)$ for $m = 0$. From (29), we deduce that (30) is bounded as

$$|g_n(\mathbf{x})| \le (m+1)\sqrt{\frac{\lambda_{\max}(\acute{\mathbf{R}}_m^{-1})}{\lambda_{\min}(\acute{\mathbf{R}}_m^{-1})}} \qquad \forall\, n \in \{1, 2, \ldots, N\}.$$

Note that the GMSC is parameterized only by $\acute{\mathbf{R}}_m^{-1}$ and is thus a semiparametric detector.

B. Isotropic Sign Correlator

The ISC is essentially the GMSC but with $\acute{\mathbf{R}}_m^{-1} = \mathbf{I}_{m+1}$, i.e., it is the GMSC for isotropic αSGN(m). This results in the simplified expression

$$g_n(\mathbf{x}) = x_n \sum_{i=\max(m+1,n)}^{\min(n+m,N)} \|\mathbf{x}_{i,m}\|^{-1}. \tag{31}$$

As $\lambda_{\max}(\mathbf{I}_{m+1}) = \lambda_{\min}(\mathbf{I}_{m+1}) = 1$, (31) is bounded by

$$|g_n(\mathbf{x})| \le m+1 \qquad \forall\, n \in \{1, 2, \ldots, N\}.$$

The ISC is no longer dependent on $\acute{\mathbf{R}}_m^{-1}$ and is essentially nonparametric. What makes the ISC remarkable is its outstanding performance in snapping shrimp noise (presented later on in Section VI) even though it requires no information of the noise process whatsoever. It is however dependent on the predetermined model order m.

By removing its dependence on $\acute{\mathbf{R}}_m^{-1}$, the ISC offers less computational complexity than the GMSC as no matrix operations are required and $\|\mathbf{x}_{i,m}\|$ breaks down into $m+1$ multiplications. Consequently, the runtime reduces to $\mathcal{O}(m+N)$. Moreover, by considering only the range $m+1 \le n \le N-m$, (31) reduces to

$$g_n(\mathbf{x}) = x_n \sum_{i=n}^{n+m} \|\mathbf{x}_{i,m}\|^{-1} = x_n \sum_{i=-m}^{0} \|\mathbf{x}_{n-i,m}\|^{-1}. \tag{32}$$

By employing an m-sample delay, we can implement (32) by a realizable filter, i.e.,

$$\begin{aligned} g_{n-m}(\mathbf{x}) &= x_{n-m} \sum_{i=0}^{m} \|\mathbf{x}_{n-i,m}\|^{-1} \\ &= x_{n-m}\left(h_n * \|\mathbf{x}_{n,m}\|^{-1}\right) \end{aligned} \tag{33}$$

where $*$ is the linear convolution operator and $h_n = 1\ \forall\, n \in \{0, 1, \ldots, m\}$ and is zero otherwise. We also note that

$$\|\mathbf{x}_{n,m}\|^2 = \sum_{k=0}^{m} x_{n-k}^2 = x_n^2 * h_n. \tag{34}$$

Therefore, from (33) and (34), we can implement (32) by two disjoint convolutions, i.e.,

$$g_{n-m}(\mathbf{x}) = x_{n-m}\left(h_n * \left(\frac{1}{\sqrt{x_n^2 * h_n}}\right)\right). \tag{35}$$

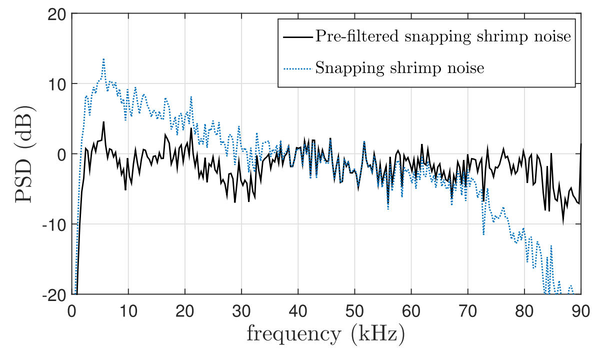

Fig. 5. Spectral densities of snapping shrimp noise with and without prefiltering.

We note that the convolution setup in (35) delays the decision in (27) by m samples.

C. Prefiltered Isotropic Sign Correlator

One notes that the ISC assumes $\acute{\mathbf{R}}_m^{-1} = \mathbf{I}_{m+1}$, which corresponds to isotropic αSGN(m). As highlighted in Section II-D, isotropic αSGN(m) has a flat PPSD. It therefore might be conducive to flatten (whiten) the PPSD of the time-series x_n before passing it through the ISC. The corresponding filter can be easily derived by expressing (6) in terms of the delay operator $\tau^{(k)}$ [22], i.e.,

$$\left(1 - \sum_{k=1}^{m} \psi_k \tau^{(k)}\right) G_n = \sqrt{\kappa} Z_n.$$

This results in the $m+1$ nonzero filter coefficients

$$v_n = \begin{cases} 1, & \text{for } n = 0 \\ -\psi_n, & \text{for } 0 < n \le m \\ 0, & \text{o.w.} \end{cases} \tag{36}$$

Alternatively, we can express (36) as the coefficient vector

$$\mathbf{v} = \begin{bmatrix} 1 \\ -\boldsymbol{\psi} \end{bmatrix} = \begin{bmatrix} 1 \\ -\mathbf{r}_m^{\mathsf{T}} \mathbf{R}_{m-1}^{-1} \mathbf{J}_m \end{bmatrix} = \begin{bmatrix} 1 \\ -\acute{\mathbf{r}}_m^{\mathsf{T}} \acute{\mathbf{R}}_{m-1}^{-1} \mathbf{J}_m \end{bmatrix} \tag{37}$$

from where we note that $\mathbf{v}$ is independent of δ.

To highlight the impact of prefiltering on snapping shrimp noise, we apply it to the data set used in Fig. 1. Both the original and output PSDs are evaluated by the Welch method [24] and plotted in Fig. 5. We consider the $m = 8$ case and $\mathbf{v}$ is evaluated from the parameters listed in Table II. Clearly, prefiltering with (36) flattens the noise PSD.

The prefiltering operation requires $\acute{\mathbf{R}}_{m-1}^{-1}$ for computation. However, it can take advantage of the ISC's simpler form. We term the resulting detector as the pISC. Let $\mathbf{y} = [y_1, y_2, \ldots, y_N]^{\mathsf{T}}$ such that $y_n = x_n * v_n$, then from (31), the pISC's nonlinearity is given by

$$g_n(\mathbf{y}) = y_n \sum_{i=\max(m+1,n)}^{\min(n+m,N)} \|\mathbf{y}_{i,m}\|^{-1}. \tag{38}$$

Furthermore, (27) needs to be updated to

$$T(\mathbf{y}) = \sum_{n=1}^{N} g_n(\mathbf{y})\bar{s}_n \tag{39}$$

where $\bar{s}_n = s_n * v_n$. The convolution setup in (35) can be extended to the pISC by replacing x_n with y_n.

D. Prefiltered Sign Correlator

As explained in Section III-B the SC assumes IID noise samples. Consequently, within the α-stable framework, the SC is optimized for WSαSN. As the latter also exhibits a flat PPSD, it may be advantageous to apply the pISC's prefiltering here as well. The resulting time-series, $y_n \ \forall \ n \in \{1, 2, \ldots, N\}$ can then be substituted for x_n in (14) to get

$$T(\mathbf{y}) = \sum_{n=1}^{N} \texttt{sign}(y_n)\bar{s}_n \tag{40}$$

where $\bar{s}_n = s_n * v_n$. We term this scheme as the pSC.

VI. Simulation Results

We now compare the performance of our proposed detectors and benchmark them against the SC and the LLR detector for αSGN(m). We employ $P_{\text{FA}} = 10^{-4}$ and $N = 1000$ in all our simulations. The transmitted signal is a linear chirp of bandwidth 18 kHz centered at either $f_c \in \{25, 54\}$ kHz. The received samples are generated by immersing the signal in either the snapping shrimp noise data set (sampled at 180 kHz) introduced in Section II-D or αSGN(4). Monte Carlo simulations are subsequently performed to determine the detectors' performance. Thresholds are determined from test statistics computed over Monte Carlo iterations under $\mathcal{H}_0$ and are equated to the $(1 - P_{\text{FA}})$th order statistic. For αSGN(4), Table II is used to construct $\acute{\mathbf{R}}_4$. Moreover, we employ $\alpha = 1.5$, as this represents severe snapping shrimp noise [5]. The αSGN(4) realizations are generated via the method outlined in [21]. On a final note, all parametric detectors are given perfect knowledge of the αSGN(4) model's parameters and are thus clairvoyant. However, in the case of snapping shrimp noise, the model's parameters are initially estimated from the noise data. In Section VI-A, we present simulation results for the additive noise case, while the acoustic channel is considered in Section VI-B.

A. Additive Noise Model

In Fig. 6, we analyze the performance of all detectors in αSGN(4) for $f_c = 25$ kHz by plotting P_{D} against SNR. The LLR detector is optimal and performs a few decibels better than the SC. All proposed detectors are clearly near-optimal. Of these the GMSC and ISC perform at par and are closest to the LLR detector's curve. We note that the pISC and pSC perform better than the ISC and SC, respectively. Therefore, prefiltering improves performance in αSGN(4). Similar trends are seen for the $f_c = 54$ kHz case in Fig. 7. However, in the latter scenario, the respective gains of the proposed detectors over the SC have increased. We also note that increasing f_c shifts the transmitted signal spectrum to a region where the noise PPSD is smaller (refer to Fig. 1). This results in an overall better performance for *all* detectors. Moreover, the GMSC now outperforms the pISC and operates almost at par with the optimal detector. Both Figs. 6 and 7 highlight the importance of exploiting memory within the noise process.

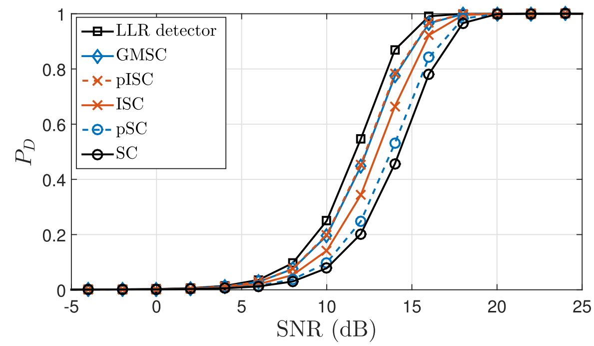

Fig. 6. Detection performance in αSGN(4) for $\alpha = 1.5$, $P_{\text{FA}} = 10^{-4}$, $N = 1000$, and $f_c = 25$ kHz.

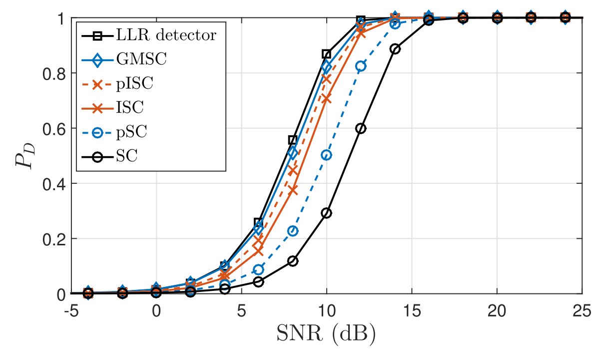

Fig. 7. Detection performance in αSGN(4) for $\alpha = 1.5$, $P_{\text{FA}} = 10^{-4}$, $N = 1000$, and $f_c = 54$ kHz.

On a side note, all proposed detectors, with the exception of the ISC require *only* $\acute{\mathbf{R}}_m$. The ISC can be interpreted as the GMSC without any knowledge of $\acute{\mathbf{R}}_m$ and therefore is essentially a nonclairvoyant GMSC, i.e., $\acute{\mathbf{R}}_m$ consists of "estimation error." In general, nonclairvoyant detection performance will depend on the estimator employed to evaluate $\acute{\mathbf{R}}_m$ and the number of samples available for estimation [14]. This in turn will cause some performance degradation in αSGN(m). However, for an asymptotically efficient estimator and a sufficient number of samples, the nonclairvoyant detectors can perform approximately similar to their clairvoyant counterparts. Moreover, analogous to the relationship between the GMSC and ISC, nonclairvoyant scenarios are depicted by the SC (for the pSC) and the ISC (for the GMSC and pISC).

In Fig. 8, we plot the performance curves in snapping shrimp noise for $f_c = 25$ kHz. Besides the SC, all detectors are built on the assumption that $m = 4$. In comparison to the curves in Fig. 6, the relative gains between the detectors are smaller. Moreover, there are a few other discrepancies as well. Most notably, the LLR detector performs *worse* than the GMSC, ISC, and pSC in the transition region but recovers at around SNR > 18

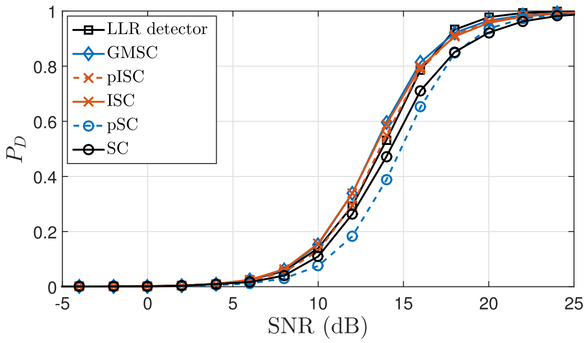

Fig. 8. Detection performance in snapping shrimp noise for $P_{\mathrm{FA}} = 10^{-4}$, $N = 1000$, and $f_c = 25$ kHz.

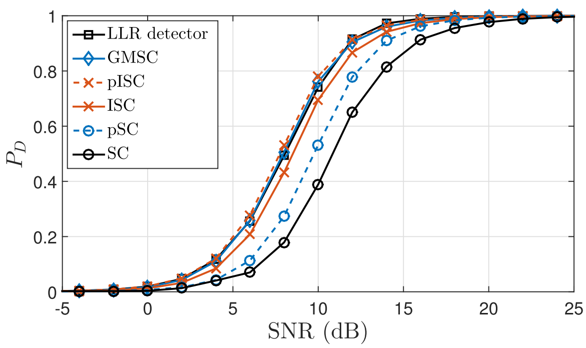

Fig. 9. Detection performance in snapping shrimp noise for $P_{\mathrm{FA}} = 10^{-4}$, $N = 1000$, and $f_c = 54$ kHz.

dB. This anomaly is attributed to the LLR's over-reliance on the αSGN(4) model, which results in adverse performance due to model mismatch. We also note that the pISC and pSC perform slightly worse than the ISC and SC, respectively, therefore implying that prefiltering actually hinders performance for our simulation settings in snapping shrimp noise. We observe that the GMSC, ISC and pISC almost perform at par with one another. Moreover, all three detectors also outperform the SC and pSC.

To highlight detection performance in snapping shrimp noise at $f_c = 54$ kHz, we present Fig. 9. Similar to Fig. 8, the LLR detector performs slightly worse than the pISC and GMSC in the transition region but recovers at high SNR. The pISC offers the best performance overall, slightly edging out the GMSC. Unlike the $f_c = 25$ kHz case, prefiltering is conducive in this scenario and offers observable gain over the ISC and SC. All other trends observed in Fig. 7 extend here as well.

To highlight the impact of selecting the model order, we simulate the ISC's performance for $m \in \{0, 1, 2, 4, 8\}$ in snapping shrimp noise for $f_c = 54$ kHz and present the results in Fig. 10. Note that for $m = 0$ the ISC is essentially the SC. By just increasing m by one, detection performance improves considerably. Moreover, for our considered values of m, we observe that increasing m offers better but increasingly smaller gain. This justifies employing small m for practical purposes and is in line with findings in our previous works [6], [11]. Though not shown here, similar trends were noted for $f_c = 25$ kHz.

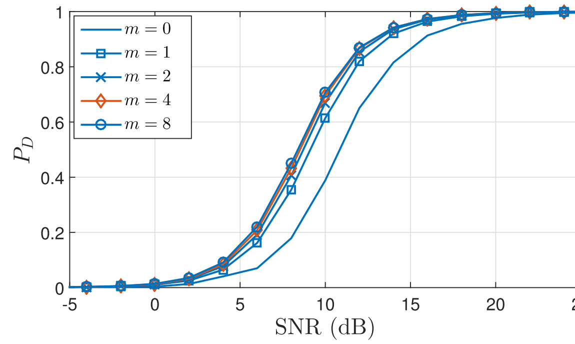

Fig. 10. Impact of m on the ISC in snapping shrimp noise for $P_{\mathrm{FA}} = 10^{-4}$, $N = 1000$, and $f_c = 54$ kHz.

TABLE III
SUMMARY OF ALL DETECTORS

Detector	Computational Complexity	Required Parameters	Gain over the SC
LLR	$\mathcal{O}(m^2 N)$	$\theta, \alpha, \delta, \acute{\mathbf{R}}_m$	3.9 dB
GMSC	$\mathcal{O}(m^2 + N)$	$\acute{\mathbf{R}}_m$	3.7 dB
ISC	$\mathcal{O}(m + N)$	m	2.9 dB
pISC	$\mathcal{O}(m + N)$	$\acute{\mathbf{R}}_m$	3.9 dB
pSC	$\mathcal{O}(m + N)$	$\acute{\mathbf{R}}_m$	1.9 dB
SC	$\mathcal{O}(N)$	–	0.0 dB

The gains are evaluated for snapping shrimp noise, for $P_{\mathrm{D}} = 0.9$, $P_{\mathrm{FA}} = 10^{-4}$, $N = 1000$, $f_c = 54$ kHz and a transmitted linear chirp of bandwidth 18 kHz.

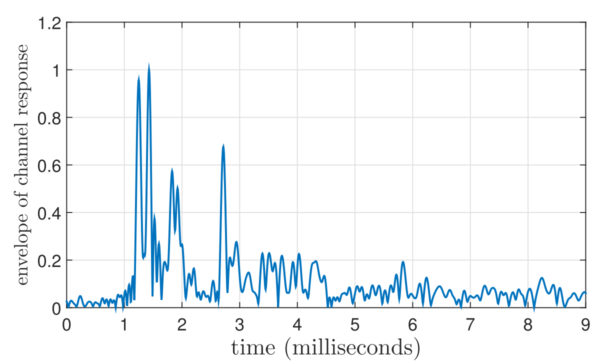

Fig. 11. Envelope of a bandpass underwater acoustical channel centered at $f_c = 25$ kHz and of bandwidth 18 kHz.

We conclude this section by listing down a summary of all detectors in Table III. The relative performance gain over the SC is also tabulated for the case of snapping shrimp noise for the parameters $f_c = 54$ kHz, $P_{\mathrm{D}} = 0.9$, $P_{\mathrm{FA}} = 10^{-4}$, and $N = 1000$.

B. *Underwater Acoustical Channel and Additive Noise*

Until now, we have only provided simulation results that do not consider the underwater acoustical channel. To analyze the performance of our proposed detectors in such a scenario, we consider the bandpass (real) channel impulse response, the envelope of which is plotted in Fig. 11. The corresponding spectra is nonzero within the interval 16–34 kHz. The baseband version of this channel was estimated during the MISSION 2013 experiment in Singapore waters [29]. To generate the received (passband) samples, the channel was convolved with the

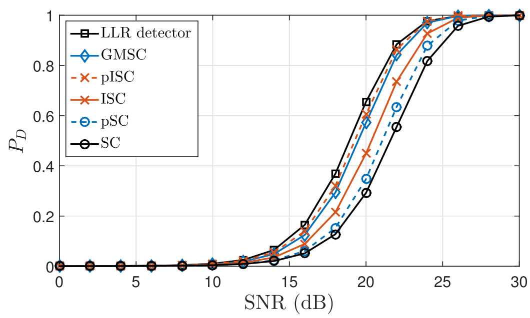

Fig. 12. Detection performance in the underwater acoustical channel with αSGN(4) for $\alpha = 1.5$, $P_{\text{FA}} = 10^{-4}$, $N = 1000$, and $f_c = 25$ kHz.

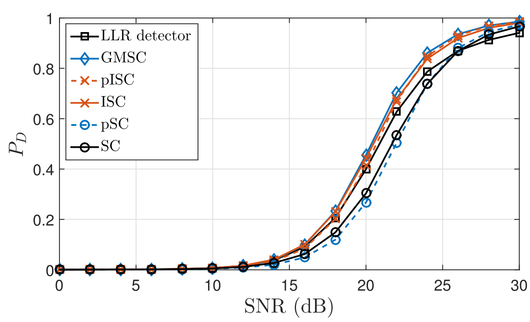

Fig. 13. Detection performance in the underwater acoustical channel with snapping shrimp noise for $P_{\text{FA}} = 10^{-4}$, $N = 1000$, and $f_c = 25$ kHz.

transmitted signal with $f_c = 25$ kHz and noise was added to it. A window of $N = 1000$ samples was selected starting from the maximum value within the impulse response. Detection performance is presented for αSGN(4) and snapping shrimp noise in Figs. 12 and 13, respectively. The relative trends in both figures remain similar to those observed in Figs. 6 and 8. However, one notes an overall deterioration in the performance of all detectors (curves shifted to the right) due to the channel. The degradation is $\sim$7 dB in both αSGN(4) and snapping shrimp noise for each detector. This is expected as the receiver has no information about the channel. Such a setup highlights a scenario where a receiver tries detecting transmitted packets via the preamble.

VII. Conclusion

We proposed a new robust detector, namely, the GMSC, that exploits memory within snapping shrimp noise. This was accomplished by modeling the noise process with αSGN(m), which is essentially a Markov impulsive process. We initially derived the LOD and found it to be ineffective in αSGN(m) at medium-to-high SNR. The GMSC was then derived by removing various penalizing terms within the test statistic. The result was shown to be bounded and therefore robust in impulsive noise. In comparison to the LLR detector, the GMSC offered significantly less computational overhead and was thus easier to implement. Moreover, the GMSC is semiparametric and does not rely on either signal strength or noise scale. We also proposed several variants, namely, the ISC, pISC, and the pSC. Detection performance was analyzed in both αSGN(4) and snapping shrimp noise, and benchmarked against the LLR detector and SC. Further still, performance was also investigated for a realization of the underwater acoustical channel. The new detectors performed extremely well in snapping shrimp noise, with a few even outperforming the LLR detector. Of all proposed schemes, the ISC is particularly attractive as it is nonparametric and yet still exploits memory within the noise samples. Furthermore, it is easier to implement than the GMSC and performs almost at par with the latter.

Appendix

A. Derivation of (17)

In [27], the LOD is derived for a general first-order Markov process. Extension to a larger order is claimed to be straight forward. Though this is true, the derivation is cumbersome. As the corresponding results are of central importance to this paper, we provide a quick derivation here.

To startoff, we drop the subscripts in (10) to get the abridged form

$$f(\mathbf{x}) = f(\mathbf{x}_m) \prod_{i=m+1}^{N} f(x_i|\mathbf{x}_{i-1,m-1}). \tag{41}$$

All PDFs on the right-hand side of (41) are αSG. Moreover, their dimensionality is highlighted by the size of their respective input argument. We assume that $N > m$ as m is small in snapping shrimp noise (refer to Fig. 1) and N is moderately high in detection scenarios. From (16), we have

$$\ell_n(\mathbf{x}) = -\frac{\frac{\partial}{\partial x_n} f(\mathbf{x})}{f(\mathbf{x})} \tag{42}$$

for all $n \in \{1, 2, \ldots, N\}$. From (41), we note that x_n is an input argument for only *some* of the right-hand side PDFs. Specifically, for $n \leq m$, we note that only the terms within $f(\mathbf{x}_m) \prod_{i=m+1}^{\min(n+m,N)} f(x_i|\mathbf{x}_{i-1,m-1})$ depend on x_n. For brevity, we denote differentiation with respect to x_n as $f'(\cdot)$, i.e., $f'(\cdot) \triangleq \partial/\partial x_n f(\cdot)$. Consequently, (42) can be simplified to

$$\ell_n(\mathbf{x}) = -\frac{\left(f(\mathbf{x}_m) \prod_{i=m+1}^{\min(n+m,N)} f(x_i|\mathbf{x}_{i-1,m-1})\right)'}{f(\mathbf{x}_m) \prod_{i=m+1}^{\min(n+m,N)} f(x_i|\mathbf{x}_{i-1,m-1})} \tag{43}$$

for $n \leq m$. From the product rule of calculus, this results in

$$\ell_n(\mathbf{x}) = -\frac{f'(\mathbf{x}_m)}{f(\mathbf{x}_m)} - \sum_{i=m+1}^{\min(n+m,N)} \frac{f'(x_i|\mathbf{x}_{i-1,m-1})}{f(x_i|\mathbf{x}_{i-1,m-1})}. \tag{44}$$

Also, as $\mathbf{x}_m = \mathbf{x}_{m,m-1}$, we have

$$\begin{aligned}\frac{f'(\mathbf{x}_m)}{f(\mathbf{x}_m)} &= \left(\frac{f(\mathbf{x}_{m+1})}{f(x_{m+1}|\mathbf{x}_{m,m-1})}\right)' \frac{f(x_{m+1}|\mathbf{x}_{m,m-1})}{f(\mathbf{x}_{m+1})} \\ &= \frac{f'(\mathbf{x}_{m+1})}{f(\mathbf{x}_{m+1})} - \frac{f'(x_{m+1}|\mathbf{x}_{m,m-1})}{f(x_{m+1}|\mathbf{x}_{m,m-1})}.\end{aligned}$$

On substituting this back in (44), we get

$$\ell_n(\mathbf{x}) = -\frac{f'(\mathbf{x}_{m+1})}{f(\mathbf{x}_{m+1})} - \sum_{i=m+2}^{\min(n+m,N)} \frac{f'(x_i|\mathbf{x}_{i-1,m-1})}{f(x_i|\mathbf{x}_{i-1,m-1})} \tag{45}$$

for $n \leq m$. Similarly, for $n > m$, the terms in (41) that depend on x_n are $\prod_{i=n}^{\min(n+m,N)} f(x_i|\mathbf{x}_{i-1,m-1})$. Therefore, we have from (42) and the product rule

$$\begin{aligned}\ell_n(\mathbf{x}) &= -\frac{\left(\prod_{i=n}^{\min(n+m,N)} f(x_i|\mathbf{x}_{i-1,m-1})\right)'}{\prod_{i=n}^{\min(n+m,N)} f(x_i|\mathbf{x}_{i-1,m-1})}\\ &= -\sum_{i=n}^{\min(n+m,N)} \frac{f'(x_i|\mathbf{x}_{i-1,m-1})}{f(x_i|\mathbf{x}_{i-1,m-1})} \end{aligned} \tag{46}$$

for all $n > m$. Both (45) and (46) are combined to get

$$\ell_n(\mathbf{x}) = \begin{cases} -\frac{f'(\mathbf{x}_{m+1})}{f(\mathbf{x}_{m+1})} \\ \quad -\sum_{i=m+2}^{\min(n+m,N)} \frac{f'(x_i|\mathbf{x}_{i-1,m-1})}{f(x_i|\mathbf{x}_{i-1,m-1})} & n \leq m \\ -\sum_{i=n}^{\min(n+m,N)} \frac{f'(x_i|\mathbf{x}_{i-1,m-1})}{f(x_i|\mathbf{x}_{i-1,m-1})} & n > m. \end{cases} \tag{47}$$

To get (17), we need to convert the conditional PDFs in (47) to their joint forms. We employ the relationship

$$\begin{aligned}\frac{f'(x_i|\mathbf{x}_{i-1,m-1})}{f(x_i|\mathbf{x}_{i-1,m-1})} &= \left(\frac{f(\mathbf{x}_{i,m})}{f(\mathbf{x}_{i-1,m-1})}\right)' \frac{f(\mathbf{x}_{i-1,m-1})}{f(\mathbf{x}_{i,m})}\\ &= \frac{f'(\mathbf{x}_{i,m})}{f(\mathbf{x}_{i,m})} - \frac{f'(\mathbf{x}_{i-1,m-1})}{f(\mathbf{x}_{i-1,m-1})}. \end{aligned} \tag{48}$$

For the $n > m$ case, we get (17) by directly substituting (48) in (47) and noting that the $i = n$ term does not depend on x_n, i.e.,

$$\sum_{i=n}^{\min(n+m,N)} \frac{f'(\mathbf{x}_{i-1,m-1})}{f(\mathbf{x}_{i-1,m-1})} = \sum_{i=n+1}^{\min(n+m,N)} \frac{f'(\mathbf{x}_{i-1,m-1})}{f(\mathbf{x}_{i-1,m-1})}.$$

A similar substitution is made for $n \leq m$, after which we invoke

$$\frac{f'(\mathbf{x}_{m+1})}{f(\mathbf{x}_{m+1})} + \sum_{i=m+2}^{\min(n+m,N)} \frac{f'(\mathbf{x}_{i,m})}{f(\mathbf{x}_{i,m})} = \sum_{i=m+1}^{\min(n+m,N)} \frac{f'(\mathbf{x}_{i,m})}{f(\mathbf{x}_{i,m})}$$

to achieve the required result.

B. Boundedness of $|\zeta_1(\mathbf{z})|$—Proving (24)

One way to determine if $|\zeta_1(\mathbf{z})|$ is bounded stems from expressing it as

$$|\zeta_1(\mathbf{z})| = \left(\frac{\|\mathbf{z}\|^2}{\|\mathbf{R}_m^{-1/2}\mathbf{z}\|^2}\right)^{1/2} \frac{|\mathbf{z}^\mathsf{T}\mathbf{d}_k^{(m)}|}{\|\mathbf{z}\|}. \tag{49}$$

From [30, p. 342], as $\|\mathbf{R}_m^{-1/2}\mathbf{z}\|^2/\|\mathbf{z}\|^2$ is the Rayleigh quotient of $\mathbf{R}_m^{-1}$, we have

$$\frac{\|\mathbf{z}\|^2}{\|\mathbf{R}_m^{-1/2}\mathbf{z}\|^2} \leq \frac{1}{\lambda_{\min}(\mathbf{R}_m^{-1})}. \tag{50}$$

This results in

$$|\zeta_1(\mathbf{z})| \leq \frac{1}{\sqrt{\lambda_{\min}(\mathbf{R}_m^{-1})}} \frac{|\mathbf{z}^\mathsf{T}\mathbf{d}_k^{(m)}|}{\|\mathbf{z}\|}. \tag{51}$$

Moreover, from the Cauchy–Schwarz inequality, we have $|\mathbf{z}^\mathsf{T}\mathbf{d}_k^{(m)}|/\|\mathbf{z}\| \leq \|\mathbf{d}_k^{(m)}\|$. On substituting this in (51), we get

$$|\zeta_1(\mathbf{z})| \leq \frac{\|\mathbf{d}_k^{(m)}\|}{\sqrt{\lambda_{\min}(\mathbf{R}_m^{-1})}}. \tag{52}$$

Further still, as $\mathbf{d}_k^{(m)} = \mathbf{R}_m^{-1}\mathbf{u}_k$, where $\mathbf{u}_k$ is the kth unit vector of dimension $m+1$, we employ properties of the Rayleigh quotient to get $\|\mathbf{d}_k^{(m)}\|^2 = \|\mathbf{R}_m^{-1}\mathbf{u}_k\|^2 \leq \lambda_{\max}(\mathbf{R}_m^{-1})$. Consequently, from (52), we get the bound

$$|\zeta_1(\mathbf{z})| \leq \sqrt{\frac{\lambda_{\max}(\mathbf{R}_m^{-1})}{\lambda_{\min}(\mathbf{R}_m^{-1})}}. \tag{53}$$

This concludes the proof.

ACKNOWLEDGMENT

The authors would like to thank K. T. Beng for acquiring the ambient noise recordings in Singapore waters, which were used in this paper. The authors would also like to thank the anonymous reviewer who suggested the elegant proof in Appendix B.

REFERENCES

[1] K. Pelekanakis and M. Chitre, "Adaptive sparse channel estimation under symmetric alpha-stable noise," *IEEE Trans. Wireless Commun.*, vol. 13, no. 6, pp. 3183–3195, Jun. 2014.

[2] M. Stojanovic and J. Preisig, "Underwater acoustic communication channels: Propagation models and statistical characterization," *IEEE Commun. Mag.*, vol. 47, no. 1, pp. 84–89, Jan. 2009.

[3] M. W. Legg, "Non-Gaussian and non-homogeneous Poisson models of snapping shrimp noise," Ph.D. dissertation, Dept. Imag. Appl. Phys., Curtin Univ. Technol., Bentley, WA, USA, 2009.

[4] J. R. Potter, T. W. Lim, and M. A. Chitre, "Ambient noise environments in shallow tropical seas and the implications for acoustic sensing," *Oceanol. Int.*, vol. 97, pp. 2114–2117, 1997.

[5] M. Chitre, J. Potter, and S.-H. Ong, "Optimal and near-optimal signal detection in snapping shrimp dominated ambient noise," *IEEE J. Ocean. Eng.*, vol. 31, no. 2, pp. 497–503, Apr. 2006.

[6] A. Mahmood and M. Chitre, "Modeling colored impulsive noise by Markov chains and alpha-stable processes," in *Proc. MTS/IEEE Oceans—Genoa*, May 2015, pp. 1–7.

[7] A. Mahmood and M. Chitre, "Temporal analysis of stationary Markov α-sub-Gaussian noise," in *Proc. MTS/IEEE Oceans—Monterey*, Sep 2016, pp. 1–6.

[8] P. Huber and E. Ronchetti, *Robust Statistics (Wiley Series in Probability and Statistics Series)*. Hoboken, NJ, USA: Wiley, 2009.

[9] J. G. Gonzalez and G. R. Arce, "Statistically-efficient filtering in impulsive environments: Weighted myriad filters," *EURASIP J. Appl. Signal Process.*, vol. 2002, pp. 4–20, Jan. 2002.

[10] A. Mahmood, "Digital communications in additive white symmetric alpha-stable noise," Ph.D. dissertation, Dept. Elect. Comput. Eng., Nat. Univ. Singapore, Singapore, Jun. 2014.

[11] A. Mahmood and M. Chitre, "Optimal and near-optimal detection in bursty impulsive noise," *IEEE J. Ocean. Eng.*, vol. 42, no. 3, pp. 639–653, Jul. 2017.

[12] A. Mahmood and M. Chitre, "Uncoded acoustic communication in shallow waters with bursty impulsive noise," in *Proc. IEEE 3rd Underwater Commun. Netw. Conf.*, Aug. 2016, pp. 1–5.

[13] A. Mahmood, H. Vishnu, and M. Chitre, "Model-based signal detection in snapping shrimp noise," in *Proc. IEEE 3rd Underwater Commun. Netw. Conf.*, Aug. 2016, pp. 1–5.

[14] S. Kay, *Fundamentals of Statistical Signal Processing: Detection Theory (Prentice Hall Signal Processing Series)*. Englewood Cliffs, NJ, USA: Prentice-Hall, 1998.

[15] J. H. McCulloch, *Numerical Approximation of the Symmetric Stable Distribution and Density*. Cambridge, MA, USA: Birkhauser Boston, Inc., 1998, pp. 489–499.

[16] C. L. Nikias and M. Shao, *Signal Processing With Alpha-Stable Distributions and Applications*. New York, NY, USA: Chapman & Hall, 1996.

[17] G. Samorodnitsky and M. S. Taqqu, *Stable Non-Gaussian Random Processes: Stochastic Models With Infinite Variance*. London, U.K.: Chapman & Hall, 1994.

[18] J. P. Nolan, *Stable Distributions—Models for Heavy Tailed Data*. Boston, MA, USA: Birkhauser, 2015, ch. 1. [Online]. Available: http://fs2.american.edu/jpnolan/www/stable/stable.html

[19] M. Chitre, J. Potter, and S. Ong, "Viterbi decoding of convolutional codes in symmetric α-stable noise," *IEEE Commun. Letters*, vol. 55, no. 12, pp. 2230–2233, Dec. 2007.

[20] J. P. Nolan, " Multivariate elliptically contoured stable distributions: Theory and estimation," *Comput. Stat.*, vol. 28, no. 5, pp. 2067–2089, 2013.

[21] A. Mahmood and M. Chitre, "Generating random variates for stable sub-Gaussian processes with memory," *Signal Process.*, vol. 131, pp. 271–279, 2017.

[22] P. Stoica and R. L. Moses, *Spectral Analysis of Signals*. Upper Saddle River, NJ, USA: Pearson Prentice Hall, 2005, vol. 452.

[23] S. Kring, S. T. Rachev, M. Höchstötter, and F. J. Fabozzi, " Estimation of α-stable sub-Gaussian distributions for asset returns," in *Risk Assessment (Contributions to Econ Series)*. Heidelberg, Germany: Physica-Verlag, 2009, pp. 111–152.

[24] P. D. Welch, "The use of fast fourier transform for the estimation of power spectra: A method based on time averaging over short, modified periodograms," *IEEE Trans. Audio Electroacoust.*, vol. 15, no. 2, pp. 70–73, Jun. 1967.

[25] A. Papoulis and U. S. Pillai, *Probability, Random Variables and Stochastic Processes*. Boston, MA, USA: McGraw-Hill, Dec. 2001.

[26] S. Kassam and J. Thomas, *Signal Detection in Non-Gaussian Noise (Springer Texts in Electrical Engineering Series)*. Berlin, Germany: Springer-Verlag, 1988.

[27] D. M. Hummels and J. Ying, "Locally optimal detection of unknown signals in non-Gaussian Markov noise," in *Proc. 34th Midwest Symp. Circuits Syst.*, May 1991, vol. 2, pp. 1098–1101.

[28] A. Mahmood, M. Chitre, and M. A. Armand, "On single-carrier communication in additive white symmetric alpha-stable noise," *IEEE Trans. Commun.*, vol. 62, no. 10, pp. 3584–3599, Oct. 2014.

[29] M. Chitre and K. Pelekanakis, "Channel variability measurements in an underwater acoustic network," in *Proc. Underwater Commun. Netw. Conf.*, Sep. 2014, pp. 1–4.

[30] G. Strang, *Linear Algebra and Its Applications*. Pacific Grove, CA, USA: Brooks/Cole, 2006.

Ahmed Mahmood (S'11–M'14) received the B.Eng and M.Eng degrees in electrical engineering from the National University of Sciences and Technology, Islamabad, Pakistan, in 2006 and 2009, respectively, and the Ph.D. degree in communications engineering from the Department of Electrical and Computer Engineering, National University of Singapore (NUS), Singapore, in 2014.

In 2014, he joined the Acoustic Research Laboratory, NUS, where he is currently a Research Fellow and a Research Lead. His current research interests include underwater acoustical communications, robust signal processing, channel modeling, estimation and detection theory, and error correction coding for impulsive noise.

Dr. Mahmood was a reviewer for several technical journals, including the IEEE TRANSACTIONS ON COMMUNICATIONS, the IEEE TRANSACTIONS ON SIGNAL PROCESSING, IEEE JOURNAL OF OCEANIC ENGINEERING, IEEE COMMUNICATIONS LETTERS, and IEEE SIGNAL PROCESSING LETTERS. He was the TPC Chair for International Conference on Underwater Networks and Systems 2016 (WUWNet'16). He is currently with the IEEE Singapore AUV Challenge Committee.

Mandar Chitre (S'04–M'05–SM'11) received the B.Eng. and M.Eng. degrees in electrical engineering from the National University of Singapore (NUS), Singapore, in 1997 and 2000, respectively, the M.Sc. degree in bioinformatics from the Nanyang Technological University, Singapore, in 2004, and the Ph.D. degree in underwater communication from NUS, in 2006.

From 1997 to 1998, he was with the Acoustic Research Laboratory, NUS. From 1998 to 2002, he headed the technology division of a regional telecommunications solutions company. In 2003, he rejoined ARL, initially as the Deputy Head (Research) and is currently the Head of the laboratory. He holds a joint appointment with the Department of Electrical and Computer Engineering, NUS, as an Associate Professor. His current research interests include underwater communications, underwater acoustical signal processing, and marine robotics.

Dr. Chitre was with the technical program committees of the IEEE OCEANS, International Conference on Underwater Networks and Systems (WUWNet), DTA, and Offshore Technology Conference and has was a Reviewer for numerous international journals. He was the Chairman of the Student Poster Committee for IEEE OCEANS'06 in Singapore, the Chairman for the IEEE Singapore AUV Challenge 2013, and the TPC Chair for the WUWNet'16 Conference. He is currently the IEEE Ocean Engineering Society Technology Committee Co-Chair of Underwater Communication, Navigation, and Positioning.

Hari Vishnu (S'04–M'13) received the B.Tech. degree in electronics and electrical engineering from National Institute of Technology Calicut, Kozhikode, India, in 2008 and the Ph.D. degree in computer engineering from the Nanyang Technological University (NTU), Singapore, in 2013.

Since 2013, he has been with the Acoustic Research Laboratory, National University of Singapore, Singapore. He is currently a Research Lead. His research interests include active sonar, bioacoustics, acoustic propagation modeling, robust signal processing, and machine learning for underwater applications. His Ph.D. research involved development of improved underwater signal processing algorithms. These included detection and localization, vector sensor processing and robust processing in non-Gaussian noise, acoustic modeling, and Bayesian parameter estimation.

Dr. Vishnu was a reviewer for several reputed international journals. He currently serves as the Secretary of the IEEE Singapore AUV Challenge Committee and the IEEE Oceanic Engineering Society, Singapore Chapter.